Characterization of GaN HEMT Low-Frequency Dispersion Through a Multiharmonic Measurement System

Antonio Raffo, *Member, IEEE*, Sergio Di Falco, *Student Member, IEEE*, Valeria Vadalà, *Student Member, IEEE*, and Giorgio Vannini, *Member, IEEE*

***Abstract*—In this paper, the experimental characterization of low-frequency dispersion (i.e., long-term memory effects) affecting microwave GaN HEMTs is carried out by adopting a new nonlinear measurement system, which is based on low-frequency multiharmonic signal sources. The proposed setup, which has been fully automated by a control software procedure, enables given source/load device terminations at fundamental and harmonic frequencies to be synthesized. Different experimental results are provided to characterize well-known effects related to low-frequency dispersion (e.g., knee walkout and drain current collapse) and to demonstrate the validity of assumptions commonly adopted for electron device modeling.**

***Index Terms*—Field-effect transistors (FETs), microwave amplifiers, semiconductor device measurements, semiconductor device modeling, time-domain measurements.**

I. Introduction

ELECTRON device traps and thermal effects (i.e., low-frequency dispersion phenomena) represent a critical issue in microwave device nonlinear modeling and circuit design, especially when new technologies (e.g., GaN) are investigated. Although latest technologies are not ready for large-scale production, they strongly attract the interest of the research community. As a consequence, it is necessary to provide modeling and design tools also in the presence of important low-frequency dispersion effects, which would be unacceptable for practical applications. An example is provided by the GaN technology: although preliminary devices showed a 70% current collapse under dynamic operation, GaN technology and related topics have immediately dominated the most important microwave conferences and journals due to the GaN promising performance.

When dealing with the empirical characterization of electron device low-frequency dispersion a widely adopted approach is represented by pulsed *I/V* setups [1]. Although pulsed measurements have the unique capability of providing iso-thermal and iso-dynamic device characteristics, they exhibit different critical aspects. Conventional pulse generators can easily satisfy their specifications, in terms of duration and amplitude of the pulse, in a 50-Ω environment. However, such an operating condition is not representative for a microwave transistor, which is a nonlinear dynamic load. As a matter of fact, this leads to critical and device-dependent calibration procedures. Moreover, pulsed waveforms present a very small energetic content (ideally zero), a condition that is very far from microwave circuit actual operation.

An alternative measurement system based on sinusoidal excitation was presented in [2], and extended in [3], where two signal sources were exploited to obtain automatic load synthesis capability. In particular, in [3], the electron device *resistive core* (i.e., the part of the intrinsic device, which is subject to the most important dispersive, thermal and nonlinear effects and is responsible for output power delivery) was characterized and exploited, in conjunction with a lookup-table model of the device capacitances, to successfully design class-A/AB power amplifiers.

In this paper, the measurement system proposed in [2] and [3] is extended by adopting multiharmonic signal sources. The new setup has been fully automated by a control software procedure, which synthesizes given source and load device terminations both at fundamental and harmonic frequencies. Such a device characterization has been exploited in this work as a valuable tool to investigate GaN HEMT low-frequency dispersion effects.

High-efficiency classes of operation for power amplifiers have become strategic topics since power efficiency represents a key issue to meet the severe performance required by modern microwave systems. As is well known, more- (e.g., class B) or less-conventional (e.g., class F) high-efficiency amplifier modes [4], [5] need the appropriate source and load terminations not only at the fundamental, but also at harmonic frequencies. The setups adopted in [2] and [3], where only the fundamental harmonic component is controlled, are not useful in this context; on the contrary, the measurement system here proposed can be used for accurate *I/V* device modeling under strongly nonlinear regimes or even exploited for high-efficiency power-amplifier design by using an approach similar to the one proposed in [3].

Although high-frequency time-domain measurement systems have been largely and successfully adopted to investigate low-frequency dispersive effects and high-efficiency operation (e.g., [5]–[15]), the new idea of exploiting a low-frequency setup to

Manuscript received December 18, 2009; revised May 18, 2010; accepted June 04, 2010. Date of publication August 09, 2010; date of current version September 10, 2010. This work was supported in part by the Italian Ministry of Instruction, University and Research (MIUR).

The authors are with the Department of Engineering, University of Ferrara, 44100-Ferrara, Italy (e-mail: antonio.raffo@unife.it; sergio.difalco@unife.it; valeria.vadala@unife.it; giorgio.vannini@unife.it).

Color versions of one or more of the figures in this paper are available online at http://ieeexplore.ieee.org.

Digital Object Identifier 10.1109/TMTT.2010.2058934

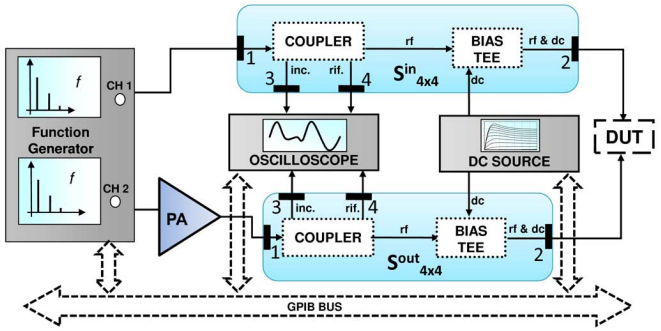

Fig. 1. Block diagram of the proposed measurement system.

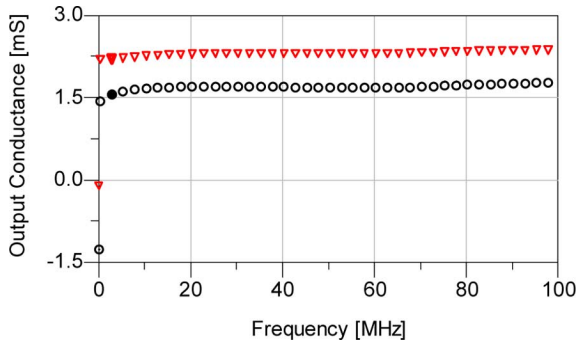

Fig. 2. 400-μm GaN HEMT output conductance versus frequency for two different bias conditions: $V_{g0} = -3$ V, $V_{d0} = 20$ V (triangles), and $V_{g0} = -2$ V, $V_{d0} = 25$ V (circles). The filled symbols represent the output conductance value at 2 MHz.

directly investigate the device resistive core behavior [3] under realistic load lines provides, as will be shown in the following, a number of advantages.

II. New Large-Signal Measurement Setup

The architecture of the proposed large-signal low-frequency measurement system is shown in Fig. 1. In particular, the function generator has two 50-Ω channels that can independently provide arbitrary waveforms in the frequency range (1 mHz–120 MHz). To overcome the power limitation of the function generator, a 30-W power amplifier is cascaded to the channel devoted to the device output port excitation. Two wideband (10 kHz-400 MHz) dual directional couplers monitor the device-under-test (DUT) incident and reflected waves, which are acquired by means of a four-channel digital oscilloscope (4 GSamples/s). A high-resolution (4 μV; 20 fA) and accurate (V: 0.05%, I: 0.2%) dc source provides the bias for the DUT. To ensure dc and RF path isolation, two wideband (200 kHz–12 GHz) bias-tees are used.

In order to characterize only the device resistive core [3], it is necessary to operate at frequencies where the dynamic effects associated to charge storage variations and/or finite transit times can be neglected. Moreover, it is of primary interest to characterize device response above the cutoff of low-frequency dispersion (this is why pulsed setups exploit very short pulse duration). To this end, a 2-MHz fundamental frequency has been found adequate for the electron devices considered in this work. The validity of such a choice has been verified on the basis of S-parameter measurements carried out, in the frequency range (300 kHz–98 MHz), by exploiting a low-frequency vector network analyzer (VNA) (HP4195A). More precisely, Fig. 2 shows the measured output conductance for a 0.25-μm GaN HEMT device having a periphery of 400 μm, under two different bias conditions corresponding, respectively, to class-A and class-AB operation. In the same figure, the output conductance dc values are also reported to highlight that frequency variations in the range (2 MHz–98 MHz) are negligible. This confirms that a 2-MHz frequency is sufficient to operate above the cutoff of low-frequency dispersion coherently with the large number of papers (e.g., [16]) devoted to microwave device characterization where pulsed measurements with a pulsewidth of 500 ns or longer have been adopted.

In the selected frequency range, all the measurement setup components satisfy linear nondistortion conditions. This greatly simplifies the setup calibration procedure, which practically consists in the experimental characterization of the two four-port networks ($S^{\text{in}}_{4\times4}$ and $S^{\text{out}}_{4\times4}$) shown in Fig. 1. The characterization can be carried out by adopting the same procedure that has been fully detailed in [2] or, alternatively, by simply exploiting a low-frequency VNA (HP4195A).

By observing the block diagram shown in Fig. 1, it is evident that the proposed setup looks similar to a large-signal network analyzer (LSNA) [8]–[14]. The similarity becomes more pronounced by considering the LSNA architecture recently proposed by Mesuro Limited[1] [15], which is based on a sampling oscilloscope operating at microwave frequencies. Nevertheless, the setup proposed in this paper is specifically oriented to the characterization of dispersion affecting *I/V* dynamic characteristics. In this context, the low-frequency operation makes the required instrumentation inexpensive and avoids complex calibration procedures, which are essentially related to microwave operation [10], [17].

The measurement setup has been automated via an IEEE488 standard interface by means of a commercial instrument automation software. The graphical user interface (Fig. 3) of the control software enables measurements to be carried out in an automated way: the user can define the dc parameters, in terms of a bias grid (voltage or current) and related compliances, in accordance with the device safe operating area. The two channels of the signal generator, which sets the incident signals applied to the device ports, are controlled in an independent way: for each one, the user can define the fundamental frequency component and the number of harmonics. For a maximum level of flexibility, the user can arbitrarily define amplitude and phase for each spectral component.

III. Experimental Results

To highlight the capabilities of the described setup, large-signal measurements, oriented to high-efficiency power amplifier design [4]–[6], were carried out on a 0.7×800 μm^2 GaN HEMT. The bias condition was $V_{g0} = -4$ V and $V_{d0} = 25$ V (class B operation), whereas the incident signals applied at the

[1]Mesuro Limited, Cardiff, U.K. [Online]. Available: http://www.mesuro.com/

Fig. 3. Graphical user interface of the control software.

TABLE I
MAGNITUDE AND PHASE OF THE RF SIGNALS APPLIED TO THE DUT

Gate Incident Signal Phasors	*Frequency*	*Drain Incident Signal Phasors*
2\85°	2 MHz	6.2\-107°
0	4 MHz	2.3\152°
0	6 MHz	1.3\-110°

DUT ports are summarized in Table I in terms of their spectral components.

Fig. 4(a) shows the dynamic load line corresponding to the described measurement condition. It is evident that a typical high-efficiency operation is obtainable by simply controlling the amplitude and phase of the fundamental, second, and third harmonic components of the incident signal at the drain terminal of the DUT. In this particular case study, an output power of 2.2 W was measured, corresponding to a drain efficiency of 74%.

At a few megahertz, the input port of a field-effect transistor (FET) behaves as an open circuit until the off-state of the gate–source diode is preserved. This greatly simplifies the control of the gate incident signal. In the present case, a 4-V amplitude of the gate input voltage is imposed, which leads to a peak-value equal to 0 V. In Fig. 4(a), the device dc characteristics ($-4\ \text{V} \leq V_{g0} \leq 0\ \text{V}$) are shown: it is well evident that, due to the current collapse [7], the load-line is not able to dynamically reach the drain-current values corresponding to the dc characteristic at $V_{g0} = 0$ V. Moreover, an important knee walkout [7], [9] is present. It is evident how the proposed setup effectively characterizes the limits of the given technology.

Time-domain waveforms at the drain port of the electron device are shown in Fig. 4(b). The dynamic current looks like an half-wave rectified sine-wave, which is different from zero where the drain voltage is minimum, according with high-efficiency power-amplifier operation modes [4], [5]. In this context, the capability of synthesizing a given load-line and get information on suitable drain and gate terminations for the device resistive core can be exploited not only for *I/V* modeling under realistic operation, but also for amplifier design following approaches like the one proposed in [3].

It is of interest to investigate some commonly accepted assumptions related to power amplifier design. Computer-aided design (CAD)-based amplifier design techniques are based on

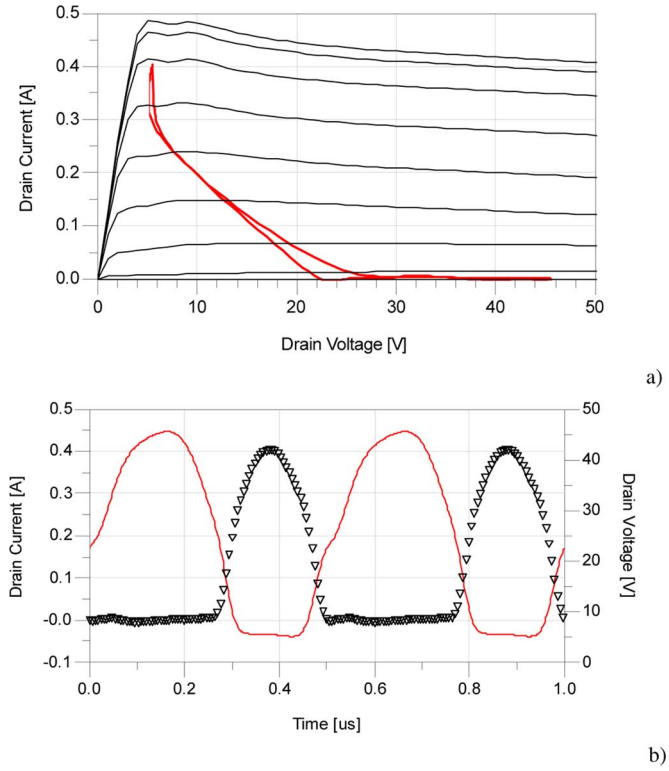

Fig. 4. Measurements performed by exploiting the proposed large-signal measurement system on a 800-μm GaN HEMT device, quiescent condition ($V_{g0} = -4\ \text{V}, V_{d0} = 25\ \text{V}$). (a) The measured load line is superimposed to dc characteristics ($-4\ \text{V} \leq V_{g0} \leq 0\ \text{V},$ step $0.5\ \text{V}$). (b) Time-domain voltage (continuous line) and current (triangles) waveforms at the device drain terminal, corresponding to the synthesized high-efficiency operation.

the accurate knowledge of the device intrinsic resistive core. A clear example is provided by the Cripps' load-line theory [4], which identifies the optimum device operation by analyzing the device dc characteristics and defining the optimum loading condition as the resistance that maximizes voltage and current excursions. As a matter of fact, all amplifier design techniques, from class-A to high efficiency (e.g., class F), are *de facto* based on the definition of the optimum waveforms of the electrical quantities at the device intrinsic current source, i.e., the device resistive core. However, due to traps and thermal effects [18], [19], the transistor resistive core shows under dynamic operation a behavior that is very different with respect to the static one. The proposed setup has the unique capability of directly and exhaustively characterizing such a behavior.

As a case study we investigate the behavior of a $0.25 \times 400\ \mu\text{m}^2$ GaN HEMT under high-efficiency operation. In particular, Fig. 5 shows three different load lines providing the different performance levels reported in Table II. Also in this case, the impact of low-frequency dispersion on the device performance is well evident. The device is not able to dynamically reach the dc characteristic at $V_{g0} = 1$ V and the *I/V* knee under dynamic operation is quite far from the dc one. Both these phenomena, by limiting the drain current and voltage excursions, reduce the deliverable output power with respect to the one predictable on the basis of the dc characteristics.

By observing the load lines in Fig. 5, at a first glance it is well evident which is the best one. Efficiency and power are the worst

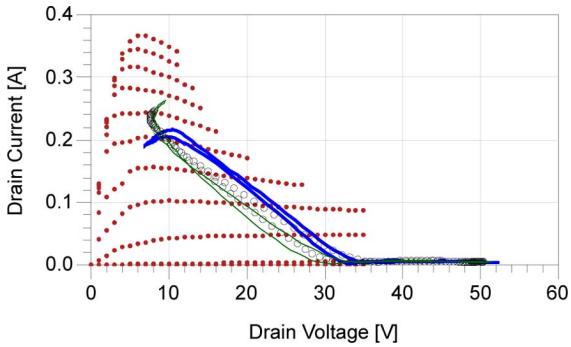

Fig. 5. Different load lines synthesized by exploiting the proposed large-signal measurement system on a 400-μm GaN HEMT device, quiescent condition ($V_{g0} = -4$ V, $V_{d0} = 30$ V). Amplitude of the gate incident signal fundamental phasor $A_g = 2.5$ V. Relative phase between gate and drain incident signal fundamental phasors $\Delta\varphi = 180°$. The measured load lines are superimposed to dc characteristics (-6 V $\leq V_{g0} \leq 1$ V, step 0.5 V).

TABLE II
PERFORMANCE RELATED TO THE DIFFERENT LOAD LINES SHOWN IN FIG. 5

Load Line	*Output Power*	*Efficiency*
Thick	1.25 W	54 %
Circles	1.64 W	60 %
Thin	1.72 W	61 %

ones for the thick load line since it involves the highest dissipation path and minimizes the drain current excursion. Similar considerations indicate that the thin load line is the best one. Such a simplicity in stating the best operating condition has to be regarded as peculiar to the proposed setup since a similar information cannot be drawn by observing extrinsic load lines carried out at microwave frequencies.

Theoretical considerations can be also carried out by observing the intrinsic drain voltage waveforms corresponding to the considered load lines; they are shown in Fig. 6 with their harmonic components. Fig. 6(a) refers to the thick load line; in this case, only the fundamental tones of the input and output incident signals have been controlled. This is evident by looking at the second and third harmonics, which assume very low amplitudes. Fig. 6(b) refers to the circles load line; in this case, the amplitude and phase of the third harmonic of the output incident signal have also been manipulated. It is evident the contribution of the third-harmonic, which, being out-of-phase with respect to the fundamental one, raises the amplifier performance according to class-F operation [5]. Nevertheless, class-F operation requires also a short loading condition at the second harmonic, this condition can be simply obtained by also manipulating the second harmonic of the output incident signal. The result is shown in Fig. 6(c), where the amplitude of the second harmonic has been halved.

In Table III, the load impedances synthesized for the different load lines are reported. The impedances at the second and third harmonics differ from 50 Ω although, for the thick load line, only the fundamental phasor of the incident signals has been exploited. This can be explained by considering that the values in Table III refer to the DUT planes and account for the non-idealities of the measurement setup (e.g., 30-W power amplifier

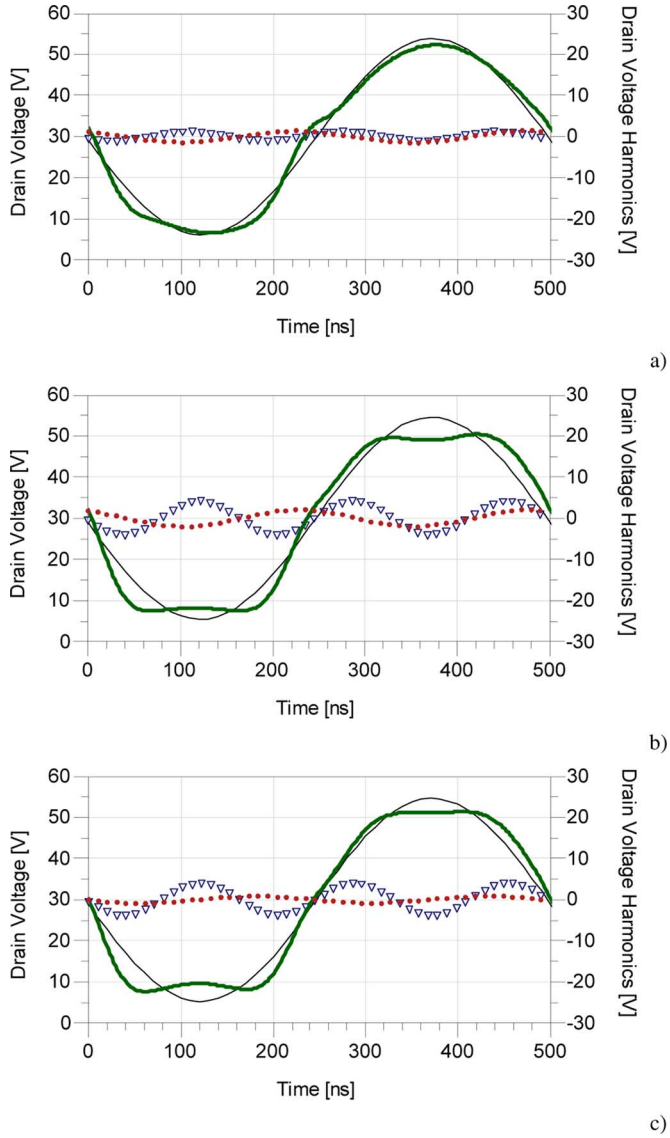

Fig. 6. Measurements performed by exploiting the proposed large-signal measurement system on a 400-μm GaN HEMT device, quiescent condition ($V_{g0} = -4$ V, $V_{d0} = 30$ V). Time-domain voltage waveform (bold line) and its harmonic components (fundamental—fine line, second harmonic—dots, and third harmonic—triangles) corresponding to the three load lines reported in Fig. 5. (a) Thick line. (b) Circles. (c) Thin line.

TABLE III
SYNTHESIZED LOAD TERMINATIONS FOR THE DIFFERENT LOAD LINES SHOWN IN FIG. 5

Load Line	*Fundamental*	*2nd Harmonic*	*3rd Harmonic*
Thick	219 – i*19 Ω	36 + i*13 Ω	47 + i*20 Ω
Circles	182 – i*11 Ω	37 + i*13 Ω	349 – i*47 Ω
Thin	177 – i*10 Ω	1 + i*15 Ω	481 – i*94 Ω

output impedance, attenuation, and delay provided by the signal paths). By looking at the impedance values in Table III, it is evident how the impedances synthesized for the thin load line are the nearest ones to the ideal class-F amplifier behavior (i.e., a short circuit at the second harmonic and an open circuit at the third harmonic).

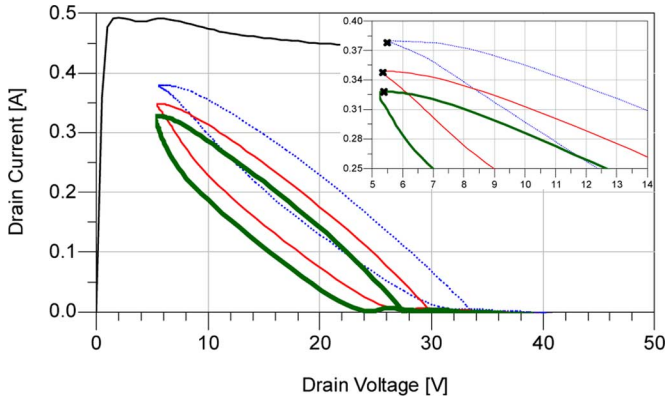

Fig. 7. Measurements performed by exploiting the new large-signal measurement system on a 800-μm GaN HEMT device, quiescent condition $V_{d0} = 25$ V and $V_{g0} = -3$ V (dotted line), $V_{g0} = -4$ V (continuous thin line), $V_{g0} = -5$ V (continuous thick line). The measured load lines are superimposed to dc characteristics at $V_{g0} = 0$ V. The crosses in the enlarged view within the inset correspond to the same instantaneous voltage pair ($v_g = 0$ V, $v_d = 5.4$ V).

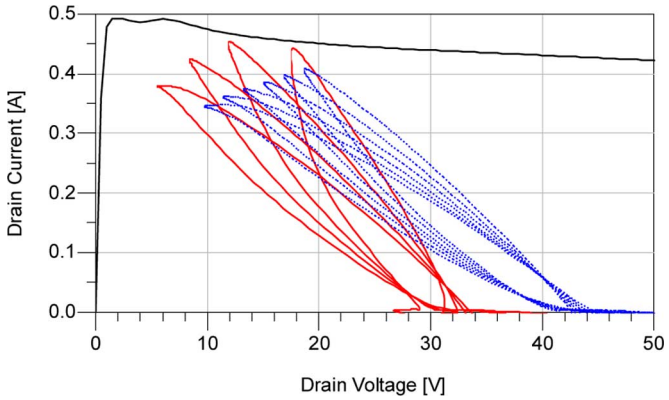

Fig. 8. Measurements performed by exploiting the new large-signal measurement system on a 800-μm GaN HEMT device, quiescent condition $V_{g0} = -3$ V and $V_{d0} = 25$ V (continuous lines), $V_{d0} = 35$ V (dotted lines). Amplitude of the gate incident signal phasor $A_g = 1.5$ V. Relative phase between gate and drain incident signal phasors $\Delta\varphi = 180°$. Different load lines are obtained by varying the amplitude of the output incident signal phasor. Measurements are superimposed to dc characteristics at $V_{g0} = 0$ V.

Measurements carried out by adopting the proposed setup, besides representing a valid tool for the design of power amplifiers, may result extremely useful in the identification phase of nonlinear electron device models. As a matter of fact, the operating conditions exploited in the identification phase are *privileged* in terms of the accuracy that the model can guarantee. As a consequence, nonlinear models extracted by adopting measurements under actual device operations unquestionably offer an higher level of accuracy.

The proposed measurement setup can be effectively used for in-depth investigation of the complex mechanisms related to low-frequency dispersion. For example, the low-frequency measurements shown in Fig. 7, carried out on a 0.7×800 μm^2 GaN HEMT, highlight the current collapse dependence on the average value of the gate voltage V_{g0}. The crosses in the enlarged view within the inset correspond to the same values of the instantaneous voltages ($v_g = 0$ V, $v_d = 5.4$ V); if low-frequency dispersion were not present, the same instantaneous current value (corresponding to the dc one) should be measured. Instead, it is well evident that as the quiescent gate voltage V_{g0} moves into the off state region, the instantaneous drain current goes down.

Moreover, also the knee walkout [7], [9] can be simply characterized. In Fig. 8, different measurement sets are reported to characterize such a phenomenon; measurements were carried out with different drain voltage quiescent conditions and setting the amplitude of the input incident signals in order to dynamically reach the value $v_g = 0$ V. It is well evident how the knee region is subject to a shift as the average value of the drain voltage increases.

By adopting the proposed characterization technique, more complex device behavior can be investigated, which can be particularly useful for discussing and defining assumptions typically adopted in the framework of nonlinear modeling. To this end, a 0.25-μm GaN HEMT device having a periphery of 150 μm, biased under class-A operation ($V_{g0} = -2$ V, $V_{d0} = 25$ V), was considered. In particular, the device was excited with very different waveform shapes, under the constraint of dynamically reaching the 0-V gate voltage value. The incident signals applied to the DUT input port are shown in terms of their spectral components (Table IV), and corresponding time-domain voltage waveforms [see Fig. 9(a)].

TABLE IV
MAGNITUDE AND PHASE OF THE INCIDENT SIGNALS APPLIED TO THE DUT INPUT PORT

Sine	*Half-sine*	*Composite*	*Frequency*
1\101°	0.58\70°	0.14\-91°	2 MHz
0	0.31\140°	0.58\127°	4 MHz
0	0.08\-150°	0.38\86°	6 MHz

The phase of the incident signals applied at the DUT output port have been set to achieve a 180° displacement with respect to the input signal (such a choice corresponds to a resistive-like load line), whereas the corresponding amplitudes were properly chosen to dynamically hit the device knee region. The corresponding load lines, evidencing the knee walkout, are shown in Fig. 9(b). The crosses in the enlarged view within the inset correspond, for the different load lines, to dynamic points having the same value of the instantaneous gate voltage ($v_g = 0$ V): it is evident that these points trace a unique dynamic characteristic. This confirms the empirical results presented in [7] and the theoretical assumption adopted in [18] and [19]: when no important deviations influence the device thermal state (this is true under class A due to the low-efficiency operation involved), the trapping state can be assumed univocally defined by the average values of the voltages applied at the device ports and no dependence is observed on the voltage waveforms.

The results provided in this paper could be indirectly obtained also by means of high-frequency time-domain measurement systems [6]–[15]. Nevertheless two reasons make the proposed characterization technique preferable when electron device low-frequency dispersion is dealt with. The first one is that parasitic and reactive effects, under high-frequency operation, tend to hide the response of the intrinsic "algebraic" part of the device (i.e., the resistive core), and the second one is the simplicity and definitely low cost of the proposed measurement technique.

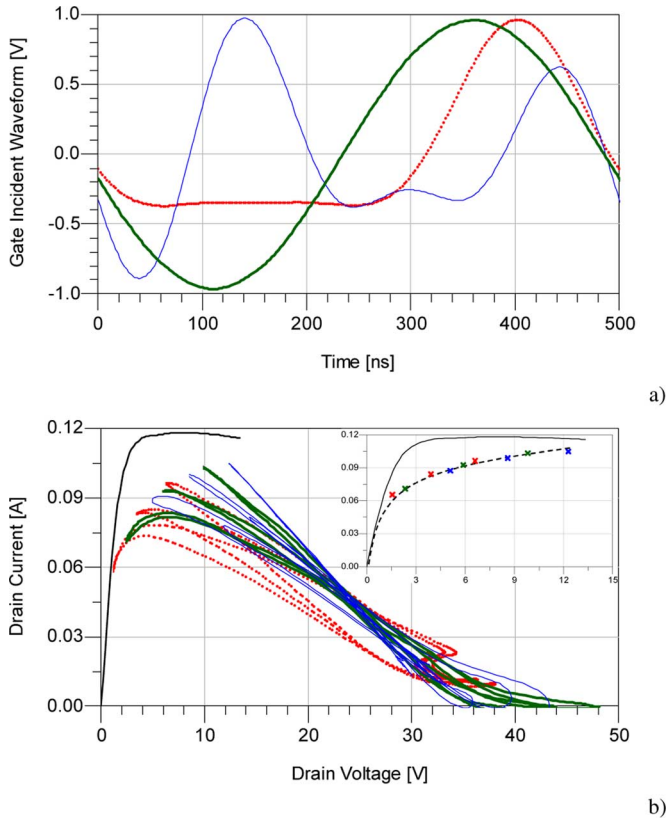

Fig. 9. Measurements performed on a 150-μm GaN HEMT by exploiting the proposed large-signal measurement system, quiescent condition ($V_{g0} = -2$ V, $V_{d0} = 25$ V). (a) Time-domain voltage waveforms at the device gate port. (b) Measured load lines. Three load lines are shown for the same gate voltage condition (thin, thick, and dotted lines) by varying the amplitude of the output incident signal phasors. Also the dc characteristic for $V_{g0} = 0$ V is shown.

IV. Conclusion

In this paper, an extensive characterization of low-frequency dispersion affecting GaN HEMTs has been carried out. In particular, a new multiharmonic measurement system specifically devoted to the investigation and characterization of low-frequency dispersion has been proposed. By exploiting different experimental examples, the unique capabilities of providing useful information for device characterization, modeling, and circuit design have been definitely demonstrated.

References

[1] J. Rodriguez-Tellez, T. Fernandez, A. Mediavilla, and A. Tazon, "Characterization of thermal and frequency-dispersion effects in GaAs MESFET devices," *IEEE Trans. Microw. Theory Tech.*, vol. 49, no. 7, pp. 1352–1355, Jul. 2001.

[2] A. Raffo, A. Santarelli, P. A. Traverso, M. Pagani, G. Vannini, and F. Filicori, "Accurate modelling of electron device *I/V* characteristics through a simplified large-signal measurement setup," *Int. J. RF Microw. Comput.-Aided Eng.*, vol. 15, no. 5, pp. 441–452, Sep. 2005.

[3] A. Raffo, F. Scappaviva, and G. Vannini, "A new approach to microwave power amplifier design based on the experimental characterization of the intrinsic electron-device load line," *IEEE Trans. Microw. Theory Tech.*, vol. 57, no. 7, pp. 1743–1752, Jul. 2009.

[4] S. C. Cripps, *RF Power Amplifiers for Wireless Communication*. Norwood, MA: Artech House, 1999.

[5] P. Colantonio, F. Giannini, and E. Limiti, *High Efficiency RF and Microwave Solid State Power Amplifiers*. New York: Wiley, 2009.

[6] P. Colantonio, F. Giannini, E. Limiti, and V. Teppati, "An approach to harmonic load– and source–pull measurements for high-efficiency PA design," *IEEE Trans. Microw. Theory Tech.*, vol. 52, no. 1, pp. 191–198, Jan. 2004.

[7] P. McGovern, J. Benedikt, P. J. Tasker, J. Powell, K. P. Hilton, J. L. Glasper, R. S. Balmer, T. Martin, and M. J. Uren, "Analysis of DC–RF dispersion in ALGaN/GaN HFETs using pulsed *I–V* and time-domain waveform measurements," in *IEEE MTT-S Int. Microw. Symp. Dig.*, Long Beach, CA, 2005, [CD ROM].

[8] D. Schreurs, K. Van der Zanden, J. Verspecht, W. De Raedt, and B. Nauwelaers, "Real-time measurement of InP HEMTS during large-signal RF overdrive stress," in *Proc. Eur. Gallium Arsenide Relat. III–V Compounds Appl. Symp.*, Amsterdam, The Netherlands, 1998, pp. 545–550.

[9] P. J. Tasker, "Practical waveform engineering," *IEEE Microw. Mag.*, vol. 10, no. 7, pp. 65–76, Dec. 2009.

[10] T. van den Broeck and J. Verspecht, "Calibrated vectorial nonlinear-network analyzers," in *IEEE MTT-S Int. Microw. Symp. Dig.*, San Diego, CA, 1994, pp. 1069–1072.

[11] J. M. Horn, J. Verspecht, D. Gunyan, L. Betts, D.E. Root, and J. Eriksson, "X-parameter measurement and simulation of a GSM handset amplifier," in *Proc. Microw. Integr. Circuit Conf.*, Amsterdam, The Netherlands, 2008, pp. 135–138.

[12] J. Verspecht, D. Gunyan, J. Horn, X. Jianjun, A. Cognata, and D. E. Root, "Multi-tone, multi-port, and dynamic memory enhancements to PHD nonlinear behavioral models from large-signal measurements and simulations," in *IEEE MTT-S Int. Microw. Symp. Dig.*, Honolulu, HI, 2007, pp. 969–972.

[13] F. De Groote, J.-P. Teyssier, J. Verspecht, and J. Faraj, "High power on-wafer capabilities of a time domain load–pull setup," in *IEEE MTT-S Int. Microw. Symp. Dig.*, Atlanta, GA, 2008, pp. 100–102.

[14] D. Vye, "Fundamentally changing nonlinear microwave design," *Microw. J.*, vol. 53, no. 3, pp. 22–44, Mar. 2010.

[15] D. McCarthy and W. Arceneaux, "Greener wireless: Non-linear analysis applied to wireless device characterization," *Microw. J.* Apr. 2009 [Online]. Available: http://www.mwjournal.com/Resources/TechLib.asp

[16] W. Ciccognani, F. Giannini, E. Limiti, P. E. Longhi, M. A. Nanni, A. Serino, C. Lanzieri, M. Peroni, P. Romanini, V. Camarchia, M. Pirola, and G. Ghione, "GaN device technology: Manufacturing, characterization, modelling and verification," in *Proc. IEEE 14th Microw. Tech. Conf.*, Prague, Czech Republic, 2008, pp. 1–6.

[17] D. Williams, P. Hale, and K. A. Remley, "The sampling oscilloscope as a microwave instrument," *IEEE Microw. Mag.*, vol. 8, no. 4, pp. 59–68, Aug. 2007.

[18] A. Santarelli, F. Filicori, G. Vannini, and P. Rinaldi, "Backgating model including self-heating for low-frequency dispersive effects in III–V FETs," *Electron. Lett.*, vol. 34, no. 20, pp. 1974–1976, Oct. 1998.

[19] A. Raffo, V. Vadalà, D. M. M.-P. Schreurs, G. Crupi, G. Avolio, A. Caddemi, and G. Vannini, "Nonlinear dispersive modeling of electron devices oriented to GaN power amplifier design," *IEEE Trans. Microw. Theory Tech.*, vol. 58, no. 4, pp. 710–718, Apr. 2010.

Antonio Raffo (S'04–M'07) was born in Taranto, Italy, in 1976. He received the M.S. degree (with honors) in electronic engineering and Ph.D. degree in information engineering from the University of Ferrara, Ferrara, Italy, in 2002 and 2006, respectively.

Since 2002, he has been with the Engineering Department, University of Ferrara, where he is currently a Contract Professor of Electronic Instrumentation and Measurement. His research activity is mainly oriented to nonlinear electron device characterization and modeling and circuit-design techniques for nonlinear microwave and millimeter-wave applications.

Dr. Raffo is a member of the Italian Association for Electrical and Electronic Measurements and the IEEE MTT-11 Technical Committee.

Sergio Di Falco (S'08) was born in Licata (AG), Italy, in 1983. He received the M.S. degree in electronic engineering from the University of Ferrara, Ferrara, Italy, in 2008, and is currently working toward the Ph.D. degree at the University of Ferrara.

In 2009, he joined the Engineering Department, University of Ferrara. His research activity is mainly oriented to nonlinear characterization and modeling of microwave electron devices and hybrid microwave integrated circuit (HMIC) and monolithic microwave integrated circuit (MMIC) design.

Valeria Vadalà (S'07) was born in Reggio Calabria, Italy, in 1982. She received the M. S. degree (with honors) in electronic engineering from the "Mediterranea" University of Reggio Calabria, Reggio Calabria, Italy, in 2006 and the Ph.D. degree in information engineering from the University of Ferrara, Ferrara, Italy, in 2010.

She is currently with the Department of Engineering, University of Ferrara. Her research interests include nonlinear electron–device characterization and modeling for microwave applications.

Giorgio Vannini (S'87–M'92) received the Laurea degree in electronic engineering and Ph.D. degree in electronic and computer science engineering, from the University of Bologna, Bologna, Italy, in 1987 and 1992, respectively.

In 1993, he joined the Department of Electronics, University of Bologna, as a Research Associate. From 1994 to 1998, he was with the Research Centre on Electronics, Computer science and Telecommunication Engineering, National Research Council (CSITE), Bologna, Italy, where he was responsible for MMIC testing and the Computer-Aided Design (CAD) Laboratory. In 1998, he joined the University of Ferrara, Farrara, Italy, as an Associate Professor, and since 2005, as a Full Professor of electronics. He is currently Head of the Engineering Department. During his academic career, he has been a Teacher of applied electronics, electronics for communications and industrial electronics. He was a cofounder of the academic spin-off Microwave Electronics for Communications (MEC). He has coauthored over 180 papers devoted to electron device modeling, computer-aided design techniques for MMICs, and nonlinear circuit analysis and design.

Dr. Vannini is a member of the Gallium Arsenide Application Symposium (GAAS) Association. He was the recipient of the Best Paper Awards presented at the 25th European Microwave Conference, GAAS98 Conference, and GAAS2001 Conference.